DENTAL MATERIALS 37 (2021) 1350–1357

Available online at www.sciencedirect.com

ScienceDirect

journal homepage: www.intl.elsevierhealth.com/journals/dema

Structural and elemental characterization of glass and ceramic particles for bone surgery

Saara V. Sirkiä[a,*], *Miho Nakamura*[b], *Syeda Qudsia*[c], *Minna Siekkinen*[d], *Jan-Henrik Smått*[c], *Jouko Peltonen*[c], *Terhi J. Heino*[e], *Leena Hupa*[d], *Pekka K. Vallittu*[a,f]

[a] *Department of Biomaterials Science and Turku Clinical Biomaterials Centre - TCBC, Institute of Dentistry, University of Turku, Lemminkäisenkatu 2, 20520 Turku, Finland*
[b] *Medicity Research Laboratory, Faculty of Medicine, University of Turku, Tykistökatu 6, 20520, Turku, Finland*
[c] *Laboratory of Molecular Science and Engineering, Åbo Akademi University, Porthansgatan 3-5, 20500 Turku, Finland*
[d] *Johan Gadolin Process Chemistry Centre, Åbo Akademi University, Biskopsgatan 8, 20500 Turku, Finland*
[e] *Institute of Biomedicine, Faculty of Medicine, University of Turku Kiinamyllynkatu 10, 20520 Turku, Finland*
[f] *City of Turku, Welfare Division, Turku, Finland*

ARTICLE INFO

Article history:
Received 20 January 2021
Accepted 2 June 2021

Keywords:
Bioceramics
Bioactive glass
Bioglass
Ion-Release
Physicochemical properties
Characterization

ABSTRACT

Objective. Clinically used bioceramics have been characterized previously with different kinds of methods and comparison of results have proven to be difficult due to varieties of the material properties of interest. Therefore, in this study we compared clinically commonly used bioceramics of hydroxyapatite and carbonate apatite, two bioactive glasses 45S5 and S53P4, and alumina with respect of properties which according to the present knowledge are significant for bone biology.

Methods. Physicochemical properties of the materials were characterized by various methods. Attenuated Total Reflectance Fourier Transform Infrared (ATR-FTIR) was used to analyze the material vibrational features. X-ray Power Diffraction (XRD) was used to characterize the material crystal structure and scanning electron microscopy-energy-dispersive x-ray analysis (SEM-EDXA) was used to evaluate the morphology and size of the materials and to calculate their oxide content. The dissolution behavior of the materials, ion release and pH changes in Tris buffer in a continuous flow-through reaction for 24-hours were determined. The change of the surface of the bioactive glasses by interfacial reaction during the Tris immersion was examined and the thickness of the surface reaction layer of the materials was studied.

Abbreviations: CAP, carbonateapatite; HAP, hydroxyapatite; Alumina, Al_2O_3; XRD, X-ray power diffraction; ATR-FTIR, Attenuated Total Reflectance Fourier Transform Infrared; SEM-EDXA, Scanning Electron Microscopy- Energy-Dispersive X-ray Analysis; ICP-OES, inductively coupled plasma optical emission spectrometry; Tris, 2-amino-2-hydroxymethyl-propane-1,3-diol.

* *Corresponding author at*: Department of Biomaterials Science, Institute of Dentistry, University of Turku, Lemminkäisenkatu 2, FI-20520 Turku, Finland.
E-mail address: savisi@utu.fi (S.V. Sirkiä).

https://doi.org/10.1016/j.dental.2021.06.004

Results. SEM examination showed that the particle morphology of BG 45S5, BG S53P4 and alumina particle's surface was smooth. The surface of HAP was porous, but also CAP showed some surface porosity. An increase in the pH of the immersion solution was observed especially for BG 45S5 and BG S53P4. HAP, CAP and alumina caused only a minor increase in pH. BGs 45S5 and S53P4 showed a rapid initial release of sodium and calcium ions, followed by the release of silicon species. Minor release of sodium ions was registered for HAP, CAP and alumina. Calcium ion release was low but constant over the experimental time while only a minor initial dissolution was measured for HAP.

Significance. The *in vitro* study showed differences in the materials' properties, which are considered to be important for biological suitability and in clinical applications, such as materials tomography, ion release and pH changes.

1. Introduction

Bioceramics such as those based on alumina, bioactive glass (BG) and hydroxyapatite are clinically used in implants for bone repair and reconstruction. Depending on their interactions with the surrounding tissue environments, bioceramics are classified as bioinert, bioresorbable and bioactive [1]. Although there are numerous studies characterizing different kinds of bioceramics *in vitro*, detailed comparative analyses of their properties are challenging due to differences in study designs and varieties of material properties of interest. For instance, fluid circulation and location of a measuring point for the property of interest in a bed of biomaterial particles can have a significant influence on the results [2,3].

A wide number of studies about alumina as surgical material for implants have been published since the 1970s. Later, alumina has become a widely clinically used bioceramic in some indications, such as orthopedic implants [4,5]. Alumina is a bioinert and biostable material. It has good biocompatibility, corrosion resistance and good mechanical properties. As an implant material, porous alumina is reported to be encapsulated by a layer of granulation tissue without direct bone contact, which is typical for materials that are not bioactive [6]. Alumina has also been used in dental implants, although it has been recently replaced by zirconia implants among the non-metallic ceramic implants [7]. Highly polished alumina has low friction coefficient and wear rate, which are essential properties for artificial joint indications [4,5].

Hydroxyapatite (HAP) has been clinically used as a bone filler as well as a coating material on biostable ceramics and metallic implants [6,8,9]. This kind of coating is one of the modification approaches used to enhance bioactivity and osteoconductivity for bone formation around the implantable biomaterials [10]. Carbonated apatite of octacalcium phosphate was synthesized to act as a bioresorbable material to better simulate the mineral of bone tissue [11–13]. Since CAP has the same composition as bone mineral [12], it can be resorbed by osteoclasts in the osteoconduction process and also by chemical dissolution [14].

BGs are bioactive and biocompatible, osteoconductive and osteoinductive, most commonly silicate glasses [15–18]. BGs have been used in bone surgery both as implants and bone filling materials [19]. Of the many BG compositions studied, BG 45S5 and BG S53P4 belong to the few that have been approved by the US FDA and European regulatory authorities for use in humans. BG's bioactivity is related with the interfacial reactions on glass surface [2]. These interfacial reactions commence immediately after the glass come into contact with the extracellular liquid in tissues [20]. In general, the dissolution and reaction rates of BGs depends on the glass composition and the composition of the surrounding solution [21]. Hench divided the reactions of BGs into 12 stages [5]. The first five reactions happen at the interface between BG and tissues and the remaining seven reactions are related to new bone formation on the BG surface. First, the alkali ions in BG are exchanged with the hydrogen ions in interfacial fluids, thus increasing the pH of the fluids. This pH increase in the interfacial solution has been reported to be one of the major factors, which induce the antibacterial effects of BGs [22]. In the second and third stages of the BG dissolution reactions, the soluble silica in the glass surface dissolves and silanols repolymerize into a silica-rich layer. Then, in the fourth and fifth stages, a layer of HAP precipitates on the glass surfaces [23]. *In vivo* the precipitation is turned to CAP. After these five steps, absorption of biochemical growth factors takes place on the surfaces and in the end, bone forms as a result of cellular interactions. Composite implants containing BG S53P4 have recently shown osteoinduction *in vitro* and *in vivo* [24].

Clinically used commercial bioceramics such as HAP and BG have good biocompatibility. There are many studies showing certain characteristic features of these bioceramics, their dissolution products and possible mechanisms of action in a biological environment. It has been suggested that the osteoinduction relates to the presence of calcium phosphates and release of ions to activate osteogenic cells to differentiate and form bone [25–28]. The biological impact of different bioceramics on bone tissue regeneration varies between the type and composition of bioceramics but no detailed comparative analyses of their properties have been performed. For example, the dissolution behavior is known to be a crucial property for several bioceramics. The aim of this study was to compare *in vitro* the characteristics of five commercial bioceramics commonly used in clinical applications. The bioceramics range

from the bioinert alumina to bioresorbable HAP and CAP as well as to the bioactive glasses 45S5 and S53P4.

2. Materials and methods

2.1. Materials

Materials which were characterized in the study are listed in Table 1.

2.2. Methods

2.2.1. Vibrational features of the characterized material using ATR-FTIR analysis

ATR-FTIR was used to analyze the vibrational features of material compounds. All materials were analyzed by using a PerkinElmer Spectrum (Version 10.4.2) spectrometer. The ATR-FTIR instrument averaged from 16 scans collected for wavenumbers from 550 cm^{-1} to 2 500 cm^{-1} at 4 cm^{-1} resolution. The software was CPU32 Main 00.09.9934 22-4-2011 and a UATR crystal combination diamond/ZnSe at 3 numbers of bounces was used.

2.2.2. Mean particle size, morphology and thickness of reaction layers of the characterized material using SEM-EDX analysis

SEM images of all materials were taken to observe the morphology of the materials and to confirm their particle sizes. The electron beam was accelerated with voltages of 15 or 20 kV The SEM used was a Leo Gemini 1530 (Carl Zeiss, Oberkochen, Germany) instrument. Particle size was analysed by ImageJ® (1.52a) bundled with Java 1.8.0_112 (64-bit) (Wayne Rasband National Institutes of Health, USA) software by setting a scale and drawing straight lines. Two to six particles were measured by four measurements, and mean particle sized was calculated using Excel (version 1808, 10730.20334). Thickness of the reaction layer of BGs after being immersed in Tris buffer for 4 h and 24 h was measured from SEM images with a magnification of 500×. Six measurements were made, and mean values were calculated.

2.2.3. Phase composition of the characterized material using XRD analysis

XRD was used to characterize the crystal structure of the materials. All materials were characterized with a Bruker D8 Discover instrument (Bruker) with Cu Kα radiation (λ = 1.54 Å). Samples were measured in the 2-theta range 5°–80°, using an increment of 0.04° and data collection of 0.2 s per step.

2.2.4. pH change and ion release materials in vitro

The *in vitro* release of ions was measured in a dynamic system in which a fresh solution of Tris buffer (2-amino-2-hydroxymethyl-propane-1,3-diol) was fed continuously (0.2 ml/min) through a bed of the sample particles at 40 °C. The pH of the (50 mM) Tris buffered solution (Trizma base, Sigma-Aldrich, pK_a 8.06) were regulated to 7.3 with 1M HCl (J-T. Baker). All sample cells were filled with materials (0.19–0.3 g) as described previously [29]. The ion concentrations and pH were measured for solution samples (4 ml) collected after the cells at the time points of 20, 40, 60, 80, 100, 120, 240, 480, and 1440 min. pH was measured with Mettle Toledo, Seven Easy electrode. For the ion analysis, 1 ml of the solution was diluted with ultrapure water (1:10) and acidified with concentrated HNO_3. The ion concentrations in the solutions were measured with Inductively Coupled Plasma Optical Emission Spectrometry (ICP-OES, PerkinElmer Optima 5300 DV, Waltham, MA, USA). The released ions were examined for silicon (LOQ 0.04), sodium (LOQ 0.2), calcium (LOQ 0.7), phosphorus (LOQ 0.03) and aluminium (LOQ 0.01). The particles were washed with ethanol, cast in epoxy resin and then cut and polished to reveal the particle cross-sections. The thickness of the reaction layers at the particle's surfaces were determined from the images taken with SEM. The oxide composition of the reaction layers that could be detected in the SEM image was analyzed using Electron Dispersive X-ray Analysis (EDXA).

3. Results

3.1. ATR-FTIR

ATR-FTIR spectra of the studied materials are shown in Fig. 1b. HAP showed strong absorbances at 563 cm^{-1}, 599 cm^{-1}, 635 cm^{-1}, 960 cm^{-1}, 1017 cm^{-1}, 1089 cm^{-1}. CAP at 563 cm^{-1}, 602 cm^{-1}, 872 cm^{-1}, 960 cm^{-1}, 1016 cm^{-1}, 1413 cm^{-1} and 1473 cm^{-1}. The spectra of BG indicated strong absorbances at 1006–1012 cm^{-1}, 906–907 cm^{-1}, and 731–746 cm^{-1} while BG 45S5 had also a strong absorbance peak at 847 cm^{-1} (Fig. 1a). Alumina showed a broad absorbance peak at 500–750 cm^{-1}.

3.2. SEM-EDXA

The SEM images in Fig. 2a show the morphology of the particles of the studied materials at 50 x and 30x magnification, the width and length of the image being 2.4 × 1.8 mm and 4.0 × 3.0 mm, respectively. The SEM images showed that the particle morphology of BG 45S5, BG S53P4 and alumina was visually similar, and the particle surface was smooth. HAP surface was especially porous, but CAP also showed some surface porosity.

The concentrations of the elements at the particle surfaces were measured with EDXA and then calculated to the oxide content, which is shown in Table 1b. The predominant oxide for BGs (S53P4 and 45S5) was silicate (SiO_2) whereas the predominant oxides for the HAP and CAP were calcium oxide (CaO) and phosphorus oxide (P_2O_5). Alumina particles demonstrated aluminium oxide (Al_2O_3) with minor quantities of sodium oxide (Na_2O). The analyzed composition and particle sizes in Table 1b are in accordance with the information provided by the manufacturers (Table 1a). The particle size in each material was measured from the SEM micrographs (Table 1b). The size of the particles was the highest in BGs, around 800 μm, while the particle size of the three different alumina samples varied between 570 and 760 μm. CAP particle size was around 450 μm, while the HAP particles were smallest, around 250 μm.

Table 1 – (a) Characterized materials of the study as specified by manufacturer (b) Oxide compositions and mean particle sizes of the studied materials based on SEM-EDX analyses.

A

Type of material	Particle size (μm)	Abbreviation	Manufacturer	LOT number
Bioactive glass 45S5[1]	500–850	BG 45S5	MO-SCI Health Care, L.L.C. 4040 HyPoint North, Rolla MO 65401 USA	257-7-1-15093
Bioactive glass S53P4[2]	500–800	BG S53P4	Mo-SCI Health Care L.L.C. 4040 HyPoint North, Rolla MO 65401 USA	19041601
Hydroxyapatite[3]	100–300	HAP	Berkeley advanced biomaterials, INC. 901 Grayson Street, Suite 101, Berkeley, CA 94710	SS20070502
Carbonated apatite[4]	300–600	CAP	Cytrans Granules GC Corporation, Tokyo, Japan	1808241
Alumina[5]	500	Al_2O_3	Duralum White (Washington mills)	NA

[1] Weight percentage of nominal composition is 24.5% Na_2O, 45% SiO_2, 6% P_2O_5, 24.5% CaO.
[2] Weight percentage of nominal composition is 23 % Na_2O, 53 % SiO_2, 4% P_2O_5, 20% CaO.
[3] Chemical structure $Ca_{10}(PO_4)_6(OH)_2$
[4] Chemical structure depend on carbonate substituting group. In Type A carbonate is substituting for OH^- and type B for PO_4^{3-}.
[5] Typical composition declared by manufacturer Al_2O_3 99.75%, Na_2O 0.25%, SiO_2 0.02%, Fe_2O_3 0.02%.

B

Materials	Particle size (diameter) μm (SD)	Compositions %					
		Na_2O	Al_2O_3	SiO_2	P_2O_5	CaO	MgO
BG S53P4	842 (52)	25.78	0.28	49.60	3.86	20.49	
BG 45S5	822 (110)	29.31	0.17	40.12	5.08	25.32	
CAP	445 (150)	5.26	1.03		39.14	54.57	
HAP	251 (24)		0.37	0.31	40.18	58.78	0.36
Alumina	574 (28)	1.74	98.26				

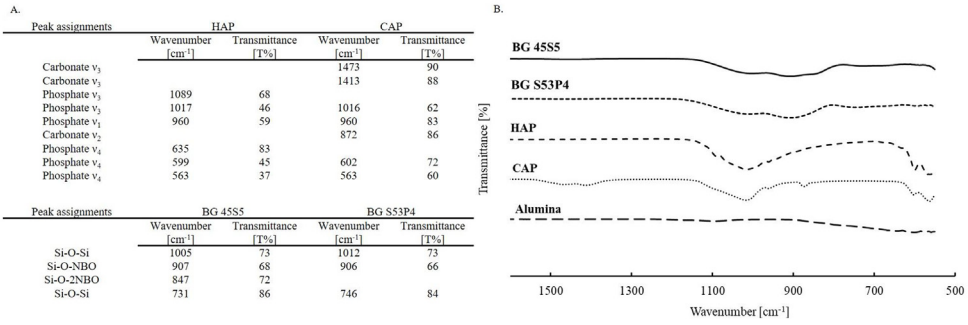

Fig. 1 – (a)ATR-FTIR peak assignments of the BG and bioresorbable materials [13,30–34] (b) ATR-FTIR spectra of the studied materials. For abbreviations, see Table 1a.

3.3. *Phase analysis*

The XRD diffractograms of the materials are shown in Fig. 2b. The XRD patterns of HAP and CAP were equivalent to the standard data for $Ca_5(PO_4)_3(OH)$ (ICDD card 00-009-0432) with some peaks matching the pattern of calcium phosphate whitlockite $Ca_3(PO_4)_2$ (ICDD card 00-055-0898). The XRD patterns of BG 45S5 and BG S53P4 showed broad peaks typical for amorphous materials.

The XRD pattern of alumina showed the main crystal phase to be corundum Al_2O_3 (ICDD card 00-010-0173), with some additional peaks which can be indexed to either beta-Al_2O_3 (ICDD card 00-051-0769), or sodium alumina ($NaAl_{5.9}O_{9.4}$) (ICDD card 00-031-1262) or diaoyudaoite ($NaAl_{11}O_{17}$) (ICDD card 00-045-1451). In addition, alumina displays a broad hump in the 10–20 2theta region, which indicates that part of the sample is amorphous.

3.4. *Ion release*

The pH and concentrations of the released ions were measured as a function of immersion time of the dissolution test. An increase of the pH of the immersion solution was shown especially for BG 45S5 and BG S53P4 within 50 to 100 min-

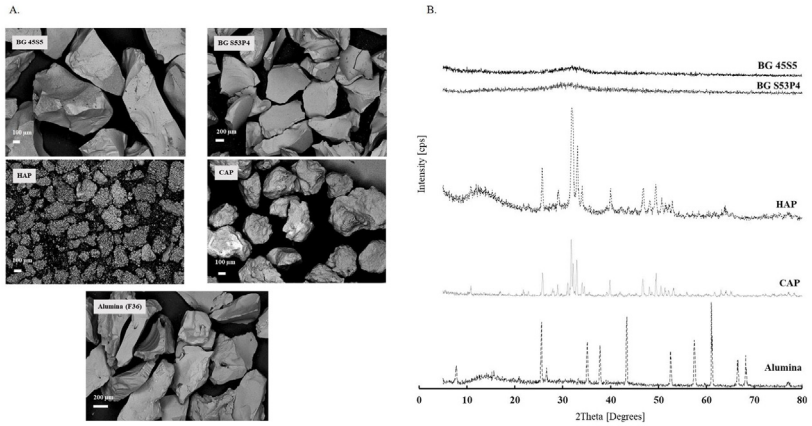

Fig. 2 – (a) SEM images of the studied materials as received/before dissolution (b) XRD patterns of the studied materials. For abbreviations, see Table 1a.

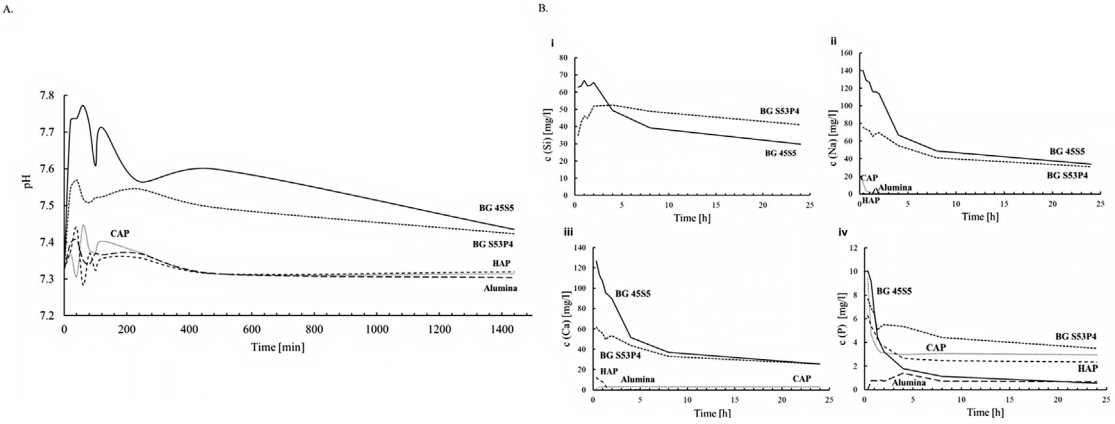

Fig. 3 – (a) pH changes of the Tris-buffer solution as functions of dissolution time in the studied materials (temperature were calculated to be at 37°C). (b) Dissolution of ions from the studied materials into Tris-buffer solution as function of time. i. silicon, ii. sodium, iii. calcium, iv. phosphorous. For abbreviations, see Table 1a.

utes, followed by a minor drop, after which the pH increased again at around the time point of 100 min (Fig. 3a). Finally, the pH of the immersion solution of the BGs gradually decreased. The three other materials, HAP, CAP and alumina caused only minor increases (0.1 pH unit) of the solution pH during the first 50 to 100 minutes of immersion. Then, the pH of the solution was on the same level as the fresh solution fed into the reaction.

Ion dissolution analyses showed clear differences between the materials (Fig. 3b). The silicate-based BGs 45S5 and S53P4 showed a rapid initial release of sodium and calcium ions, followed by the release of silicon species. Then, the ion concentrations gradually decreased but stayed at relatively high levels throughout the 24 h of experimental time. Minor initial release of sodium ions was registered for HAP, CAP and alumina, most likely due to the analyzed Na_2O impurity (Table 1b). Calcium ion release was very low but constant over the experimental time while only a minor initial dissolution was measured for HAP. The release of phosphorus from the materials was on a much lower level. After the higher initial releases during the first hours, the concentration of phosphorus decreased to clearly lower levels for BG S53P4, HAP and CAP. In contrast, the phosphorus concentration released from BG 45S5 after the first hours was near the level of quantification (LOQ) as well as for the phosphorus-free alumina during whole the test time.

3.5. *Changes in particle surface morphology*

SEM examination of particles showed formation of reaction layers at the surfaces of BG 45S5 and BG S53P4 during the 24 h of the dissolution (Fig. 4a). No reaction layer was seen by the SEM examination at HAP, CAP or alumina.

According to the SEM-EDX analysis, the thickness of the silica-rich reaction layer grew from around 15 μm at 4 h to 21 μm at 24 h for BG 45S5 (Fig. 4b). The corresponding layer thickness of BG S53P4 was 4 μm at 4 h and 12 μm at 24 h. The outermost part of the reaction layer showed the presence of calcium phosphate for both BGs.

4. Discussion

In vitro characterization of some commonly used bioceramic materials showed clear differences in properties which are typically used to describe the biological suitability of

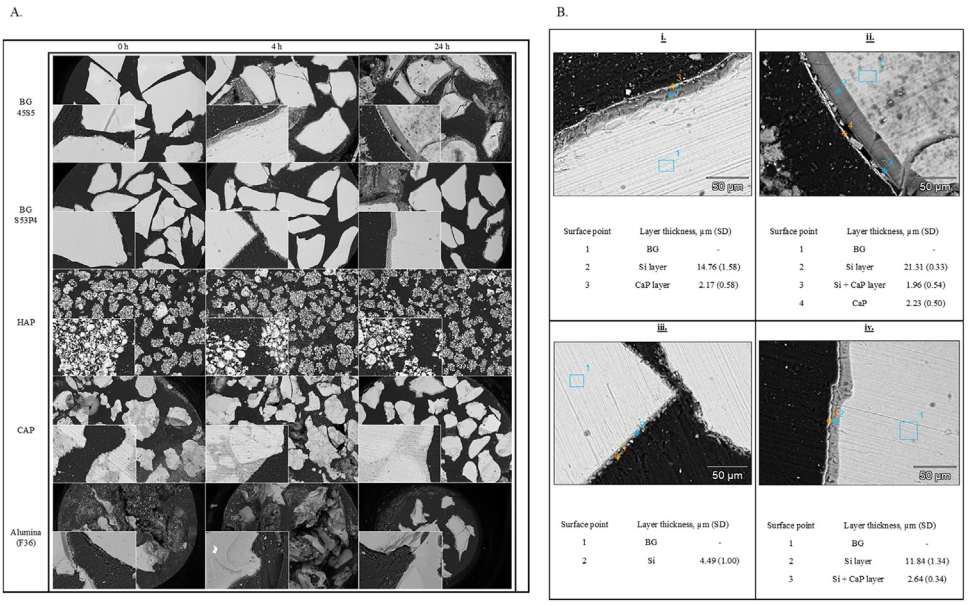

Fig. 4 – (a) SEM images of the cross-sectional surfaces of the studied materials after dissolution in continuous flow of in the Tris-buffer solution for up to 24 h at 50x and 500x (left bottom corner) magnification, the width and length of the image being 2.4 × 1.8 mm and 240 × 180 mm, respectively. (b) SEM micrographs showing the reaction layer thicknesses for BG 45S5 after 4 h (i) and 24 h (ii) and for BG S53P4 after 4 h (iii) and 24 h (iv). The EDX analyses give the elemental compositions of bulk glasses (points 1, 2) and surface layers (points 3 and 4). Si: silica rich layer; CaP: calcium-phosphate rich layer.

the materials. Material surface topography is important for cell attachment, proliferation and differentiation [11]. Bioresorbable material surface with a certain roughness and crystal structure is known to function in a desired manner for cell attachment and re-precipitation of minerals from the surrounding tissue environment [8,11]. A recent study has described hydroxyapatite amorphic surfaces as being optimal for cell behavior in a tissue environment [9].

Surface porosity is also known to increase reaction surface area and thus enhance dissolution. However, the chemical composition and crystal structure are essential parameters affecting the dissolution of bioceramics [15]. In this work, we characterized in detail the bioresorbable CAP and HAP consisting of crystalline particles and showed that the particle size was of the same order of magnitude. In addition, HAP particles of different sizes were studied.

If the material particles are small, the large surface area might lead to rapid ion release and thus to dramatic changes in the pH of the interfacial volume. These changes in the solution composition can induce toxic effects to the surrounding tissues [15,35]. On the other hand, an increase in the pH of the interfacial solution around the dissolving material can also provide antibacterial properties [22]. In fact, in optimal circumstances the implantable material which leaches ions of calcium and phosphorus, can induce ossification [36].

Material surfaces and dissolution impact molecule bonding, crystal lattice and chemical properties, the latter of which were observed by FTIR. Carbonate ions have four vibrational modes theoretically, but in this study, we observed two of these vibrational modes using ATR-FTIR [30]. Both of these observed vibrational modes also show CAP type, whether of type A or B (for explanation see Table 1a). The double bounds of the third vibrational modes at 1413 cm^{-1} and 1473 cm^{-1} CAP are attributed to be A and B type, respectively [13,31]. The synthetic materials crystallinity and solubility, as bone reformation, depend on carbon type [31]. Phosphorous ions also have four vibrational modes and the second vibrational mode is unusually weak. In this study we observed the first, third and fourth vibrational modes [30] (Fig. 1a). CAP and HAP have a hydroxyl ion vibration mode over 3 550 cm^{-1} [30,31], but we did not observe this vibrational mode, because of the scale of our wavenumbers.

BGs' atomic structure, ion release, bioactivity and solubility are influenced by glass amorphous structure and variations of glass molecule network modifiers, such as silicate (SiO_2) and phosphorous (P_2O_3) and some superstructure units. Silicate atomic network bonding changes from tetrahedral to non-bridging depending on the silicate content of the glass and other glass oxides as CaO and Na_2O. The amount of non-bridging silicate *i.e.* low glass network impacts glass degradation and ion release [34,37]. As shown in Tables 1b, BG 45S5 has a lower silicate content than BG S53P4 and our result shows that BG 45S5 has two non-bridging oxygen group per silicate at (849 cm^{-1}) [34], which is not the case for BG S53P4. Lower network formation of BG 45S5 was also seen in the dissolution test, when BG 45S5 dissolved and surface reactions happened more quickly than for BG S53P4 (Fig. 4b.). Other molecular vibrations between BG 45S5 and BG S53P4 showed similar composition bonding (Fig. 1a) [33,34]. In silicate-based bioactive glasses as BG 45S5 and BG S53P4, most of the phosphorous is present as orthophosphate [37]. Alumina had Al-O octahedral vibration bands at 500–750 cm^{-1} [32].

In this study, pH was shown to increase for all materials in the beginning but stabilized to *c.a.* pH 7.3 for the bioresorbable

and bioinert materials. For the BGs, the pH increase was a consequence of the high initial release of sodium and calcium ions. With alumina, the pH value also increased first, because alumina's sodium ion dissolved out. BG 45S5 had higher pH during Tris immersion than BG S53P4. BG 45S5 had higher pH value correlating with its higher antibacterial properties compared to BG S53P4, which has lower antibacterial properties and ion release but good osteogenic potential [20,38]. In this study, the pH curve for BGs showed two increases at time points of 50 and 100 min which were followed by a minor drop. Minor pH value variations have also been shown in previous studies [39].

BGs are osteoinductive materials by the ion dissolution. Certain ions which leach out have previously been shown to stimulate osteogenesis *via* the expression of growth factor and other genes affecting cell attachment, differentiation and proliferation [15,17,26,40]. Ion concentration in the microenvironment needs to be suitable for the osteogenic effect. Too high concentrations and too fast ion release for instance due to a large reactive BG surface area can be harmful [41]. Optimal ion concentration for osteostimulation has previously been reported to be approximately 20 ppm for silicon and 60–90 ppm for calcium [16,42]. In the present study design BGs silicon dissolution caused a higher concentration than previously. Calcium concentration with BG S53P4 was above the reported value only during the first one hour and with BG 45S5 during the first two hours. However, direct comparisons of reported ion concentrations between different studies need to be critically interpreted from the biological perspective.

Between all five characterized materials, the ion dissolution profile was different. In general, HAP, CAP and alumina showed low ion dissolution. Also, previous studies have reported HAP's low dissolution even when comparing to CAP's dissolution *in vivo* [14]. It has also been reported that osteoclasts resorb CAP more than HAP, which may influence CAP's higher osteoconductivity [11,14]. From alumina minor quantities of sodium and phosphorus dissolved relatively quickly in the beginning. These ions may be traces from the production of the particles. No signs of dissolution of aluminium ions were found.

BGs' bioactivity and osteoconductivity are based on CAP layer formation [15] and their ion dissolution profiles also showed some differences. BG 45S5 and BG S53P4 had similar dissolution curves for sodium and calcium ions, while silicon dissolved faster from BG 45S5 than from BG S53P4. Otherwise, BG S53P4 had higher silicon dissolution than BG 45S5 after four hours. Phosphorous dissolution between BGs differed. The phosphorous ions in BG 45S5 seemed to decrease inversely proportionally, while with BG S53P4 phosphorous dissolution graph had more variation and higher values during the follow-up period. Interestingly, our study showed that the dissolution of silicon was higher than in a previous study [39], which could be due to the longer dissolution time (here 24 h, previously 1 000 s). It is also possible that there are differences in particle sizes between the studies. In general, BGs dissolution and its effects on pH change were found to be in line with previous studies [16,17,38,39].

5. Conclusions

Clear differences in properties such as releasing ions, pH change and topography were observed between five commonly clinically used bioceramic materials. These properties are considered to have an impact on the biological suitability of the materials. These properties are important for choosing the optimal materials for bone surgery and instance for precise research of cell's and tissue's behaviour in a microenvironment close to the biomaterial *in vitro* and *in vivo*.

Acknowledgements

We wish to acknowledge Linus Silvander for SEM analyses and Luis Bezerra for ICP-OES analyses. Research was supported by the Academy of Finland Grant #323596.

REFERENCES

[1] Shanmugam K. Sahadevan R. 1 - Bioceramics—an introductory overview. In: Thomas S, Balakrishnan P, Sreekala MS, editors. Fundamental biomaterials: ceramics. Elsevier Ltd.; 2018. p. 1–46.
[2] Zhang D, Hupa M, Aro HT, Hupa L. Influence of fluid circulation on in vitro reactivity of bioactive glass particles. Mater Chem Phys 2008;111:497–502.
[3] Zhang D, Hupa M, Hupa L. In situ pH within particle beds of bioactive glasses. Acta Biomater 2008;4:1498–505.
[4] Christel P, Meunier A, Dorlot JM, Crolet JM, Witvoet J, Sedel L, et al. Biomechanical compatibility and design of ceramic implants for orthopedic surgery. Ann N Y Acad Sci 1988;523:234–56.
[5] Hench LL. Bioceramics: from concept to clinic. J Am Ceram Soc 1991;74:1487–510.
[6] Camilo CC, Silveira CAE, Faeda RS, Rollo de Almeida, João MD, de Moraes Purquerio B, et al. Bone response to porous alumina implants coated with bioactive materials, observed using different characterization techniques. J Appl Biomater Funct Mater 2017;15:223–35.
[7] Gross C, Bergfeldt T, Fretwurst T, Rothweiler R, Nelson K, Stricker A. Elemental analysis of commercial zirconia dental implants - is "metal-free" devoid of metals? J Mech Behav Biomed Mater 2020;107:103759.
[8] Choi G, Choi AH, Evans LA, Akyol S, Ben-Nissan B. A review: recent advances in sol-gel-derived hydroxyapatite nanocoatings for clinical applications. J Am Ceram Soc 2020;103:5442–53.
[9] Xu J, Aoki H, Kasugai S, Otsuka M. Enhancement of mineralization on porous titanium surface by filling with nano-hydroxyapatite particles fabricated with a vacuum spray method. Mater Sci Eng C 2020;111:110772.
[10] Ducheyne P, Hench LL, Kagan A, Martens M, Bursens A, Mulier JC. Effect of hydroxyapatite impregnation on skeletal bonding of porous coated implants. J Biomed Mater Res 1980;14:225–37.
[11] Anada T, Kumagai T, Honda Y, Masuda T, Kamijo R, Kamakura S, et al. Dose-dependent osteogenic effect of octacalcium phosphate on mouse bone marrow stromal cells. Tissue Eng A 2008;14:965–78.

[12] Doi Y, Koda T, Wakamatsu N, Goto T, Kamemizu H, Moriwaki Y, et al. Influence of carbonate on sintering of apatites. J Dent Res 1993;72:1279–84.
[13] Hayashi K, Munar ML, Ishikawa K. Effects of macropore size in carbonate apatite honeycomb scaffolds on bone regeneration. Mater Sci Eng C 2020;111:110848.
[14] Ishikawa K. Carbonate apatite bone replacement: learn from the bone. J Ceram Soc Jpn 2019;127:595–601.
[15] Fagerlund S, Hupa L. Melt-derived bioactive silicate glasses. In: Boccaccini Aldo R, Brauer Delia S, Hupa Leena, editors. Bioactive glasses: fundamentals, technology and applications. Royal Society of Chemistry; 2016. p. 1–26.
[16] Hupa L. 1 - Composition-property relations of bioactive silicate glasses. In: Ylänen H, editor. Bioactive glasses. Elsevier Ltd.; 2018. p. 1–35.
[17] Jones JR, Brauer DS, Hupa L, Greenspan DC. Bioglass and bioactive glasses and their impact on healthcare. Int J Appl Glass Sci 2016;7:423–34.
[18] Zheng K, Boccaccini AR. Sol-gel processing of bioactive glass nanoparticles: a review. Adv Colloid Interface Sci 2017;249:363–73.
[19] Lindfors N, Geurts J, Drago L, Arts JJ, Juutilainen V, Hyvönen P, et al. Antibacterial bioactive glass, S53P4, for chronic bone infections – a multinational study. Adv Exp Med Biol 2017;971:81–92.
[20] Vallittu PK, Närhi TO, Hupa L. Fiber glass–bioactive glass composite for bone replacing and bone anchoring implants. Dent Mater 2015;31:371–81.
[21] Nommeots-Nomm A, Hupa L, Rohanová D, Brauer DS. A review of acellular immersion tests on bioactive glasses—influence of medium on ion release and apatite formation. Int J Appl Glass Sci 2020;11:537–51.
[22] Zhang D, Leppäranta O, Munukka E, Ylänen H, Viljanen MK, Eerola E, et al. Antibacterial effects and dissolution behavior of six bioactive glasses. J Biomed Mater Res A 2010;93A:475–83.
[23] Hench LL, Andersson Ö. Chapter 3: bioactive glasses, Introduction to bioceramics. World Scientific 1993:41–62.
[24] Vallittu PK, Posti JP, Piitulainen JM, Serlo W, Määttä JA, Heino TJ, et al. Biomaterial and implant induced ossification: in vitro and in vivo findings. J Tissue Eng Regen Med 2020;14:1157–68.
[25] Björkenheim R, Strömberg G, Pajarinen J, Ainola M, Uppstu P, Hupa L, et al. Polymer-coated bioactive glass S53P4 increases VEGF and TNF expression in an induced membrane model in vivo. J Mater Sci 2017;15:9055–65.
[26] Björkenheim R, Strömberg G, Ainola M, Uppstu P, et al. Bone morphogenic protein expression and bone formation are induced by bioactive glass S53P4 scaffolds in vivo. J Biomed Mater Res B Appl Biomater 2019;107:847–57.
[27] Boonrungsiman S, Gentleman E, Carzaniga R, Evans ND, McComb DW, Porter AE, et al. The role of intracellular calcium phosphate in osteoblast-mediated bone apatite formation. Proc Natl Acad Sci 2012;109:14170–5.
[28] Shih Y, Hwang Y, Phadke A, Kang H, Hwang NS, Caro EJ, et al. Calcium phosphate-bearing matrices induce osteogenic differentiation of stem cells through adenosine signaling. Proc Natl Acad Sci U S A 2014;111:990–5.
[29] Fagerlund S, Ek P, Hupa L, Hupa M. Dissolution kinetics of a bioactive glass by continuous measurement. J Am Ceram Soc 2012;95:3130–7.
[30] Rehman I, Bonfield W. Characterization of hydroxyapatite and carbonated apatite by photo acoustic FTIR spectroscopy. J Mater Sci Mater Med 1997;8:1–4.
[31] Madupalli H, Pavan B, Tecklenburg MMJ. Carbonate substitution in the mineral component of bone: discriminating the structural changes, simultaneously imposed by carbonate in A and B sites of apatite. J Solid State Chem 2017;255:27–35.
[32] Joe IH, Vasudevan AK, Aruldhas G, Damodaran AD, Warrier KGK. FTIR as a tool to study high-temperature phase formation in sol–Gel aluminium titanate. J Solid State Chem 1997;131:181–4.
[33] Zheng K, Solodovnyk A, Li W, Goudouri O, Stähli C, Nazhat SN, et al. Aging time and temperature effects on the structure and bioactivity of gel-derived 45S5 glass-ceramics. J Am Ceram Soc 2015;98:30–8.
[34] Serra J, González P, Liste S, Serra C, Chiussi S, León B, et al. FTIR and XPS studies of bioactive silica based glasses. J Non Cryst Solids 2003;332:20–7.
[35] Monfoulet L, Becquart P, Marchat D, Vandamme K, Bourguignon M, Pacard E, et al. The pH in the microenvironment of human mesenchymal stem cells is a critical factor for optimal osteogenesis in tissue-engineered constructs. Tissue Eng A 2014;20:1827–40.
[36] Bohner M, Miron RJ. A proposed mechanism for material-induced heterotopic ossification. Mater Today 2019;22:132–41.
[37] Brauer DS, Möncke D. Chapter 3: Introduction to the Structure of Silicate, Phosphate and Borate Glasses. Bioactive Glasses 2016:61–88.
[38] Vallittu PK. Bioactive glass-containing cranial implants: an overview. J Mater Sci 2017;52:8772–84.
[39] Fagerlund S, Hupa M, Hupa L. Dissolution patterns of biocompatible glasses in 2-amino-2-hydroxymethyl-propane-1,3-diol (Tris) buffer. Acta Biomater 2013;9:5400–10.
[40] Hoppe A, Güldal NS, Boccaccini AR. A review of the biological response to ionic dissolution products from bioactive glasses and glass-ceramics. Biomaterials 2011;32:2757–74.
[41] Alm JJ, Frantzén JPA, Moritz N, Lankinen P, Tukiainen M, Kellomäki M, et al. In vivo testing of a biodegradable woven fabric made of bioactive glass fibers and PLGA80—a pilot study in the rabbit. J Biomed Mater Res B Appl Biomater 2010;93B:573–80.
[42] Hench LL. Genetic design of bioactive glass. J Eur Ceram Soc 2009;29:1257–65.